Observation and correction of non-resonant error fields in NSTX

2010 Plasma Phys. Control. Fusion 52 104003

(http://iopscience.iop.org/0741-3335/52/10/104003)

Plasma Phys. Control. Fusion **52** (2010) 104003 (14pp) doi:10.1088/0741-3335/52/10/104003

Observation and correction of non-resonant error fields in NSTX

S P Gerhardt[1], J E Menard[1], J-K Park[1], R Bell[1], D A Gates[1], B P Le Blanc[1], S A Sabbagh[2] and H Yuh[3]

[1] Princeton Plasma Physics Laboratory, Princeton, NJ, USA
[2] Department of Applied Physics and Applied Mathematics, Columbia University, New York, NY, USA
[3] Nova Photonics, Princeton, NJ, USA

Received 25 November 2009, in final form 11 March 2010
Published 7 September 2010
Online at stacks.iop.org/PPCF/52/104003

Abstract

Experiments studying non-resonant error fields have been conducted in the National Spherical Torus Experiment (NSTX) using a set of six midplane error field correction (EFC) coils. When scanning the amplitude and phase of an applied $n = 3$ field, an asymmetric response in the pulse length and plasma rotation has been observed; this indicates that there is an intrinsic $n = 3$ error field. By studying this asymmetry in plasmas with varying levels of plasma current, toroidal field and elongation, it has been concluded that the main vertical field coil is the source of the error field. Measurements of the coil shape indicate that the coil has a significant $n = 3$ distortion. The amplitude and phase of the applied $n = 3$ field, which is calculated to cancel this intrinsic error field in vacuum, are close to the experimentally derived optimal correction. Modeling of the neoclassical toroidal viscosity (NTV) also shows that the total NTV torque is minimized for the EFC coils' current and phase determined to be optimal in the experiment. Experiments have also determined that $n = 2$ error fields are small, consistent with the calculated error field from the distorted vertical field coils.

(Some figures in this article are in colour only in the electronic version)

1. Introduction

While the ideal tokamak is perfectly axisymmetric, the construction of any real tokamak will deviate to some extent from this idealization. For instance, the poloidal field coils may not be perfectly circular, or have a small tilt with respect to the horizontal [1]. Coil current feeds also disrupt the toroidal symmetry of the coil systems. The $n \neq 0$ field components that arise from these imperfections are known as error fields (EFs; here, n is the toroidal mode number). While $n = 1$ EFs are known to limit performance at both high and low β, the importance of $n > 1$ EFs has only recently begun to be understood.

In low-density plasmas, typically with low values of β, $n = 1$ resonant EFs can disrupt the plasma through a process called mode penetration [2], typically described as follows. When the plasma rotates, the external $n = 1$ field that attempts to drive the island is shielded by currents flowing on the rational surface; these currents, however, interact with the helical fields, causing a torque which slows the rotation. When that torque slows the plasma sufficiently, a loss of torque balance occurs, the shielding currents are dissipated and a large stationary island forms. More recently, theoretical attention has focused on the role of non-resonant terms in understanding the observed rotation damping and field penetration dependence on engineering parameters [3–5]. Experimentally, this process of rapid rotation damping and island formation, followed by confinement degradation and disruption, has been described in many tokamaks (see, for instance, [3, 6–15]).

At higher values of β_N, EFs can couple to any marginally stable kink-like mode, leading to an amplification of the EF [16]. Here, β_N is the value of toroidal beta ($\beta = 2\mu_0\langle p\rangle/B_T^2$) normalized by I_P/aB_T, to take into account the lowest order scaling of the beta limit in a tokamak (I_P is the plasma current, B_T is the toroidal field at the geometric center of the device, $\langle p\rangle$ is the volume average pressure and a is the minor radius defined as half the midplane width of the plasma) [17, 18]. A common manifestation of this process in high-β plasmas is known as resonant field amplification (RFA) [19, 20], where the marginally stable resistive wall mode (RWM) amplifies the externally imposed EF. This plasma amplification can play an important role in damping rotation, increasing the sensitivity of the high-β plasma to EF penetration [21] and RWMs [19, 22]. Note, however, that significant plasma modifications to the externally applied field can occur even in the low-β ohmic [23] or force-free cases [24].

Significantly less attention has been given to EFs with $n > 1$, although this trend has changed with the observation of edge localized mode (ELM) suppression with $n = 3$ applied fields in DIII-D [25, 26]. The plasma rotation damping due to the applied $n = 3$ fields was first documented in DIII-D, in experiments ostensibly designed to study the effect of helical fields on neoclassical tearing modes [27]. The braking of plasma rotation by $n = 3$ fields has been subsequently studied in National Spherical Torus Experiment (NSTX) [28] and DIII-D [29, 30]. Furthermore, it has been shown [15, 31] that in NSTX, the plasma performance can be improved by applying $n = 3$ fields that cancel an apparent intrinsic $n = 3$ EF; understanding the source of these EFs, and then correcting them, is the purpose of this paper. Note, however, that under certain conditions, $n = 3$ applied fields can actually accelerate the plasma [29, 30], demonstrating that the non-resonant fields may be beneficial for maintaining rotation in certain configurations.

These rotation dynamics are now understood to be due to neoclassical toroidal viscosity (NTV) [4, 5, 30, 32–37]. The evolution of the tokamak's toroidal rotation can be described by the equation

$$mnR\frac{\partial V_\phi}{\partial t} = \sum T + \nabla\cdot\left[mnR\left(\chi_\phi\frac{\partial V_\phi}{\partial r} - V_{\text{Pinch}}V_\phi\right)\right]. \tag{1}$$

Here, V_ϕ is the toroidal velocity, n is the ion density, m is the ion mass, χ_ϕ is the perpendicular momentum diffusivity and V_{pinch} is the momentum pinch velocity. The ΣT term represents a sum over torque densities, including those from the neutral beam injection (NBI), shielding currents at the rational surface interacting with resonant EFs [2] and NTV. Simple analytic expressions for the NTV torque can be used to illustrate some important dependences. In the low-collisionality ν regime [5]

$$T_{\text{NTV},\nu} \propto (\delta B)^2(V_\phi - V_{\phi,\text{NC}})n_i T_i^{-1/2}\omega_E^2, \tag{2a}$$

while in the higher collisionality $1/\nu$ regime, the torque is expressed as

$$T_{\text{NTV},\nu^{-1}} \propto (\delta B)^2(V_\phi - V_{\phi,\text{NC}})n_i^{-1}T_i^{5/2}\omega_E^2. \tag{2b}$$

In both cases, we see that the braking torque is proportional to the perturbed field (δB) squared; this amplitude should include the contributions from the source of the EF, any correcting fields and the field caused by shielding currents in the plasma flowing at the rational surfaces (the so-called 'plasma response') [30, 38]. Additionally, the NTV torque is proportional to the difference between the flow velocity and a neoclassical offset velocity [5] given by

$$V_{\phi,\mathrm{NC}} = k_{\mathrm{C}} \frac{1}{eZ} \frac{\mathrm{d}T_{\mathrm{i}}}{\mathrm{d}\psi}, \tag{3}$$

with $k_{\mathrm{C}} \approx 3.5$ in the $1/\nu$ regime and $k_{\mathrm{C}} \approx 0.9$ in the ν regime. This offset rotation is in the direction counter to the direction of the plasma current. When neutral beams inject significant momentum parallel to the plasma current, as in NSTX, the NTV torque is then in the direction to reduce the plasma rotation. In the other case, where the NB driven rotation is anti-parallel to the plasma current, it is possible for the non-resonant EFs to actually increase the rotation [29, 30]. Note that there exists a model for the NTV torque which smoothly bridges the two collisionality regimes, as well as including additional important particle orbit resonances [37]; this model will be used in section 4 to understand NSTX results. Further discussion of the momentum transport in NSTX plasmas can be found in [39–41].

In this paper we report detailed studies of the observation, understanding and correction of non-resonant EFs in the NSTX [42]. Section 2 provides the basic explanation of the NSTX device, including information about the coil systems which cause, and correct, the observed EF. Section 3 presents the experimental evidence regarding $n = 3$ EFs, including the process by which the main vertical field coil has been identified as the source of the EF. Section 4 uses both vacuum field and NTV calculations to demonstrate that the measured non-circularity in the vertical field coil is consistent with the experimentally determined correction. Measurements which show $n = 2$ EFs to be under the detection threshold are described in section 5, and a summary is provided in section 6.

2. The NSTX device

The cross-section of the NSTX device is shown in figure 1(a), along with the boundary shape for a discharge typical of those in this experiment. The main vertical field, which is responsible for providing radial force balance for the plasma [43], is provided by the PF-5 coils. These coils are connected in series. The main radial field, which controls the plasma elongation and vertical position, is produced by the PF-3 coils; although these two coils have independent power supplies, the current in them differs by only a few hundred amperes during the flat-top phase of these discharges. The OH coil provides a loop voltage to sustain the plasma current. The toroidal field coil is not shown in the figure.

In order to study the physics of EFs, RWM stabilization and resonant/non-resonant magnetic perturbations, NSTX is equipped with six window-frame coils mounted at the midplane outside the vessel, generating primarily a radial field [44]. These coils will be referred to as error field correction (EFC) coils in this paper. They are typically connected in an anti-series pattern, such that they are capable of making simultaneous $n = 1$ and 3 fields using the three available power supplies. As illustrated in figure 1(b), an $n = 3$ pattern is achieved when the radial field direction alternates between adjacent coils. Note that with only six coils, it is not possible to achieve arbitrary phase angles for the $n = 3$ field. However, the polarities of all coils can be reversed, leading to a 60° phase shift. Figure 1(c) shows the midplane magnetic field when the coils are connected in order to make an $n = 2$ pattern; note that this field can be rotated toroidally. The discharges utilized in this study did not use the $n = 1$ active feedback [45].

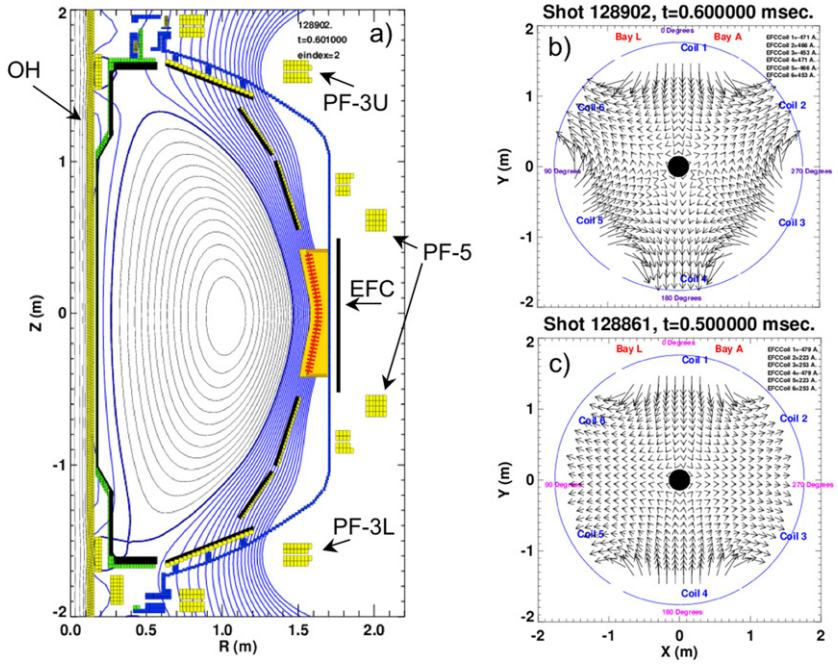

Figure 1. (*a*) NSTX coils, along with a poloidal flux plot for a discharge used in this paper, and top views of the device with arrows representing (*b*) $n = 3$ and (*c*) $n = 2$ applied field patterns.

3. Detection of the $n = 3$ EF in NSTX

The observation of $n = 3$ EFs in NSTX relies on the detection of modifications to the plasma performance as $n = 3$ fields are applied. While maximizing pulse length at high β_N as a function of the applied $n = 3$ field is one indicator of the optimal correction, we have found that a better indication comes from examining the total plasma angular momentum, defined as

$$L = \iiint_{\text{Plasma}} m_P\,(2n_D + 12n_C)\Omega R^2\,\mathrm{d}V. \tag{4}$$

Here, n_D and n_C are the density of deuterons and fully stripped carbon in the plasma, both of which are functions of position in the plasma. Ω is the fully ionized carbon toroidal rotation frequency measured by the CHERS diagnostic, and is also a function of position; no correction is made for the difference between deuterium and carbon rotation frequencies. m_P is the mass of a proton, and the integral is over the volume of the plasma.

Figure 2 shows the time evolution of discharges in two different configurations: a high plasma current case is shown in the left column, and a lower plasma current case in the right (note that additional discharges were taken in these scans, but, for the sake of clarity, are not shown). The bottom frame in each column shows the current in a representative EFC coil (coil 1), while the top frame shows the plasma current and the second frame from the top shows the evolution of β_N. Note that the band near β_N of 4 in frames (*b*) and (*f*) indicates the approximate $n = 1$ no-wall stability limit in this class of discharges. These discharges have β_N at or above the $n = 1$ limit, and so are in a stability regime where changes in the rotation can profoundly affect RWM stability [15, 19, 22, 30, 44].

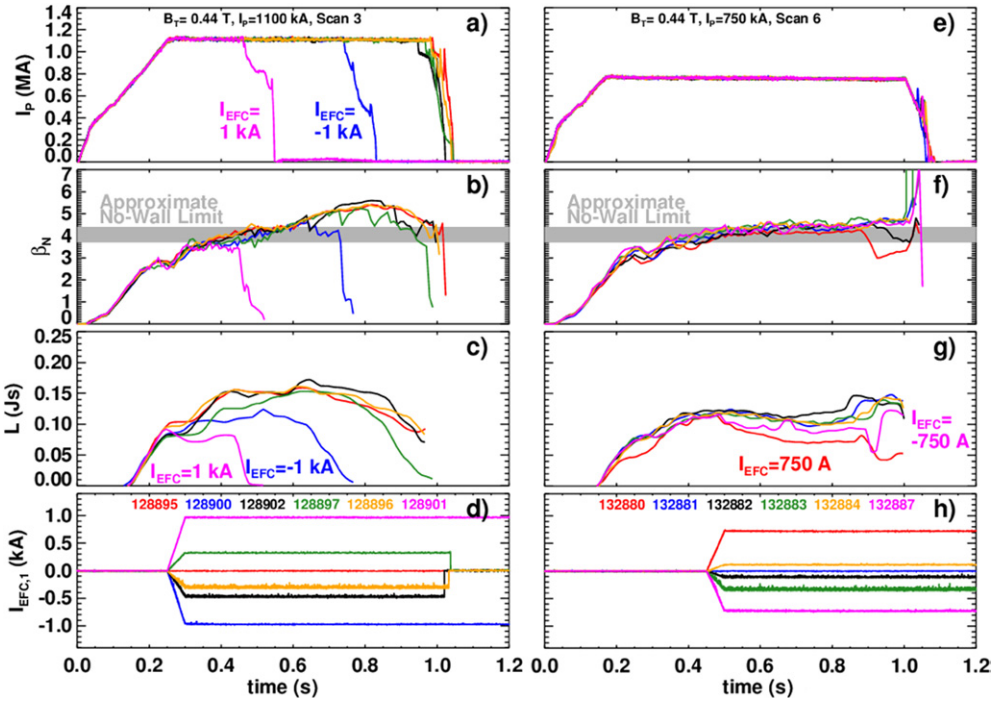

Figure 2. Plasma current (I_P), β_N, total angular momentum (L) and current in a representative EF coil (coil 1), for a set of discharges with $I_P = 1100$ kA and $B_T = 0.45$ T (left column), and $I_P = 750$ kA and $B_T = 0.45$ T (right column). The approximate $n = 1$ no-wall stability limit is indicated in the gray band of (b) and (f).

For the $I_P = 1100$ kA case on the left, a clear asymmetry in the pulse length is observed, with positive EFC coil currents of 1000 A leading to a shorter pulse than the −1000 A case. However, in the lower plasma current case in the right-hand column, all discharges have the same length, and are limited by the current in the solenoid coil. The angular momentum analysis described below, however, will clearly distinguish which applied $n = 3$ field amplitude and phase are optimal.

The third frame from the top in each column shows the time evolution of the total angular momentum of the plasma. The angular momentum traces for all the discharges in a set overlie until the $n = 3$ fields are applied; the traces then diverge. The asymmetry is once again most clear in those cases with the largest applied fields. In the left column with a larger plasma current ($I_P = 1100$ kA), the angular momentum in the discharge with $I_{EFC,1} = 1000$ is less than that in the $I_{EFC,1} = -1000$ discharge. Similarly for the $I_P = 750$ kA case in the right column, the angular momentum for the $I_{EFC,1} = -750$ A discharge is larger than for the discharge with $I_{EFC,1} = 750$. It should also be noted that for both values of plasma current (both columns), the maximum angular momentum occurs in the black traces, when there is a negative current in the representative EFC coil.

The proceeding analysis demonstrates that an EF is present, and that it can be corrected to at least some extent by applying an $n = 3$ field. It does not, however, give any indication regarding the source of the EF. The most likely sources of the EF are the TF coil, the vertical field coils (PF-5), the radial field coils (PF-3) or the solenoid and its leads. The current in the

TF coil is a directly controlled quantity. For fixed outer gap and plasma profiles, the current in the PF-5 coil scales with the plasma current. The current in the PF-3 coil will also scale with the plasma current, but can be changed by making small changes in the elongation at a fixed plasma current and outer gap. Furthermore, for a fixed I_P, the PF-3 current required to achieve a given elongation will decrease as the plasma internal inductance (l_i) is reduced; discharges with a higher plasma current generally have a lower l_i. The solenoid current will ramp through the discharge; different values of plasma current cause more ohmic flux to be used during the current ramp, leading to a scan over flat-top solenoid current as I_P is changed. The import of this discussion is that by determining the optimal correction for a series of high-β discharges with varying I_P, B_T and κ, the optimal correction can then be correlated with the currents in the coils, and the source of the EF determined. Note that other parameters, such as the triangularity, aspect ratio and outboard midplane boundary-limiter gap, are constant among the discharges in this study.

The optimal $n = 3$ correction for a given [I_P, B_T, κ] combination was determined by repeating the discharge many times with various levels of applied $n = 3$ fields; six different combinations of these parameters were used in these studies. A time window was then chosen during which the various coil currents and plasma angular momentum were averaged. The angular momentum was then fit as a function of the EFC coil current with a parabola. The peak of the parabola provides the EFC current which maximizes the plasma angular momentum; this EFC coil current is then deemed the optimal correction.

The results of this procedure are shown in figure 3, for the six scans in this study. The parabolas are in general good fits, as anticipated from the quadratic dependence of the NTV damping on the perturbation amplitude (see equations (2)). The next task is then to determine how these optimal corrections scale with the potential EF sources.

The optimal correction currents are plotted in figure 4 as a function of the various coil currents. In each frame, the data points are shown, as well as a linear fit that is forced to pass through the origin, and an arbitrary linear fit to the data. It is anticipated that these lines would overlie for the true EF source, since no correction is required when there is no EF. The slopes of the two linear fits are displayed, as well as the extrapolated EFC coil current at zero TF, OH, PF-5 or PF-3 coil current (based on the arbitrary linear fit). The correlation coefficient r^2 is also shown.

The correlation between the PF-5 (vertical field) coil current and optimal correction current is quite good ($r^2 = 0.77$). Equally importantly, the arbitrary linear fit extrapolates to essentially 0 A of EFC coil current at $I_{PF\text{-}5} = 0$. The inferred scaling of the optimal correction with the PF-5 coil current is $I_{EFC,1}/I_{PF\text{-}5} = -14\,\mathrm{A\,kA^{-1}}$.

The correlation between the optimal correction and the TF current is not as strong ($r^2 = 0.51$). Furthermore, the arbitrary linear fit extrapolates to the large fraction of the optimal correction when $I_{TF} = 0$ (~ -50 A of EFC coil current at $I_{TF} = 0$ compared with ~ -130 A for the optimal correction). Also note that a limited scan of the applied $n = 3$ field amplitude and phase was completed in a configuration with the toroidal field direction reversed. The number of discharges taken in this scan was insufficient to determine the optimal correction with accuracy necessary for inclusion in figures 3 and 4. However, it was clear that the sign of the correction did not change, further supporting the observation that the TF coil is not the source of the observed EF.

The correlations of the optimal correction with the PF-3 and OH coil currents are comparable to that with the TF. However, in both cases, the extrapolated correction current at I_{OH} or $I_{PF\text{-}3}$ of zero is far too large, and thus fails the test that there should be no correction when there is no EF.

From this analysis, we conclude that the PF-5 coil is indeed the source of the EF.

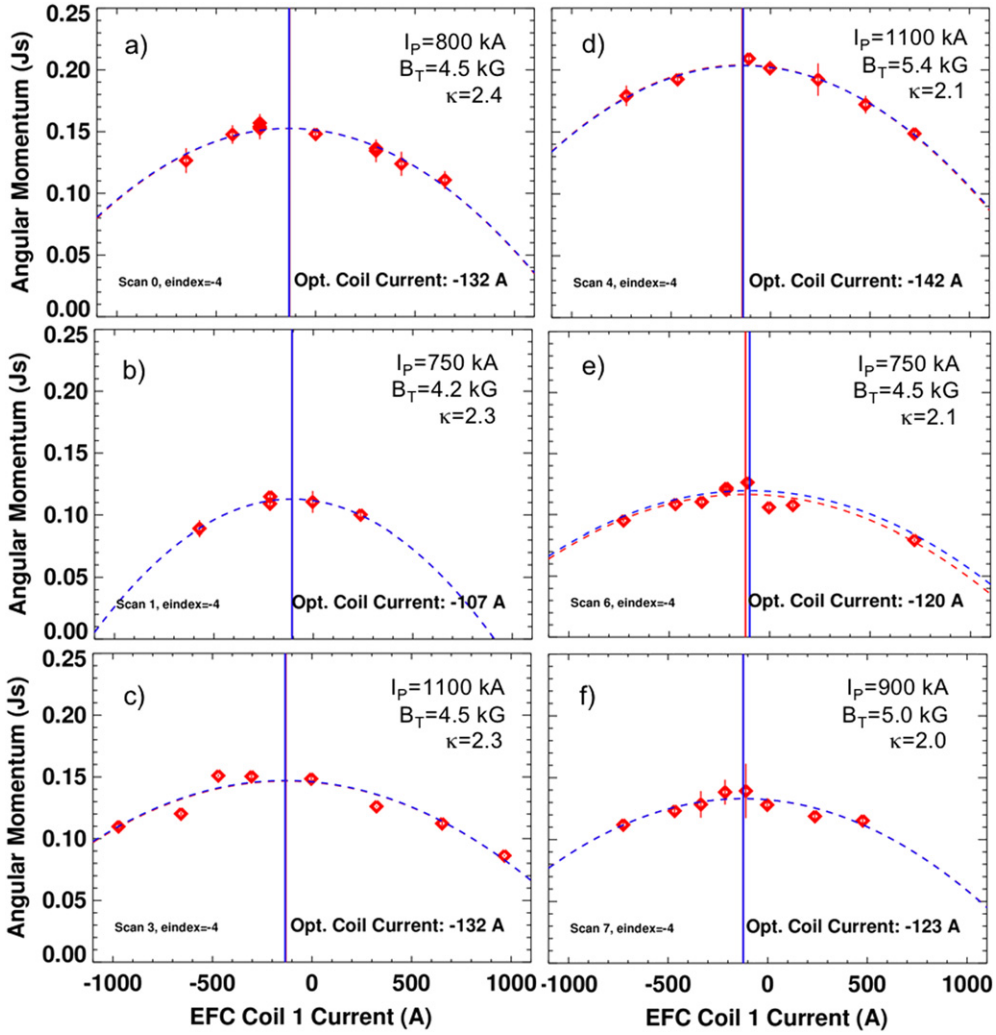

Figure 3. Angular momentum as a function of current in a representative EF coil, for the [I_P (kA), B_T (T), κ] combinations studied in this report: (*a*) [800,0.45,2.4], (*b*) [750,0.42,2.3], (*c*) [1100,0.45,2.3], (*d*) [1100,0.54,2.3], (*e*) [750,0.45,2.1] and (*f*) [900,0.5,2.0]. Each point corresponds to a single discharge.

4. Comparison with the modeled $n = 3$ EF

The measurements in the previous section were motivated by the observation that the main vertical field coil is out-of-round. In this section, we present the measured deviations of that coil shape from a circle, a calculation of the optimal vacuum correction and an optimization of the correction using the recent NTV theory.

The current centroids of the PF-5 coils were measured with a coordinate measuring arm as follows. There are a number of fiducial markers inside the NSTX vessel that are used to establish an absolute coordinate system; it is not possible, however, for the arm to both reference to those fiducials and reach points around the circumference of the coil. Instead, the radius of the vacuum vessel inner wall was measured with the arm. Then, the radial distance

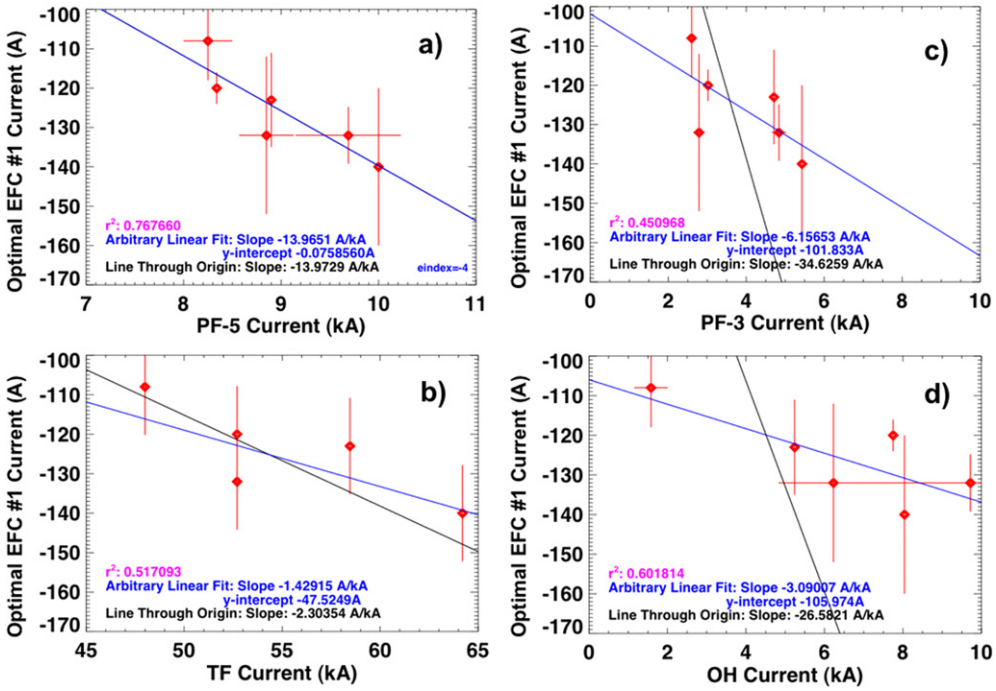

Figure 4. Optimal correction current in EFC 1 versus the current in (*a*) main vertical field coil (PF-5), (*b*) toroidal field coil (TF), (*c*) radial field coil (PF-3) and (*d*) ohmic solenoid (OH); see text for additional details.

between the outer wall of the vacuum vessel and the inside and outside radii of the coil were measured. This information, along with the thickness of the vacuum vessel, is used to calculate the toroidal variation of the coil centroid. This process was repeated for both the upper and the lower PF-5 coils.

This toroidal variation of the coil centroid is shown in figure 5, as a function of toroidal angle. The quantity shown is $100 \times (R(\phi) - \bar{R})/\bar{R}$, where $\bar{R} = 2.0\,\mathrm{m}$ is the mean coil radius. It is clear that there are up to 2 cm deviations of the coil radius from an ideal circle. Additionally, note that there are three peaks in the deviation, and that they are at approximately the same phase for the two coils. This alignment implies that there will be a significant $n = 3$ component to the EF created by this distortion.

This is confirmed to be the case in figure 6. The magnetic field due to the two PF-5 coils was calculated on a series of circles at $Z = 0$. The radial field along each circle was decomposed as $B_{R,\mathrm{S}}(R,\phi) = \sum_n C_{\mathrm{S},n}(R)\cos(\phi) + S_{\mathrm{S},n}(R)\sin(\phi)$; note that the subscript 'S' indicates the source of the EF. The amplitude and phase were then calculated as $A_{\mathrm{S},n}(R) = \sqrt{C^2_{\mathrm{S},n}(R) + S^2_{\mathrm{S},n}(R)}$ and $\phi_{\mathrm{S},n}(R) = a\tan(S_{\mathrm{S},n}(R)/C_{\mathrm{S},n}(R))$. The curve in the upper frame shows the amplitudes of the various spectral components at $R = 1.5\,\mathrm{m}$ for 10 kA in the PF-5 coils; the $n = 3$ component is clearly the largest, as expected from the curve in figure 5.

The optimal vacuum correction can be derived in a similar manner. The amplitude ($A_{\mathrm{C},n}$) and phase ($\phi_{\mathrm{C},n}$) of the correcting B_R $n = 3$ field produced by 1 A in the EFC coils are calculated as described above. The amplitude of the EFC field was then scaled by the quantity mean $(R^2 A_{S,3}(R)/R^2 A_{C,3}(R))$, where *mean* is the average over $1 < R < 1.5$. These radial

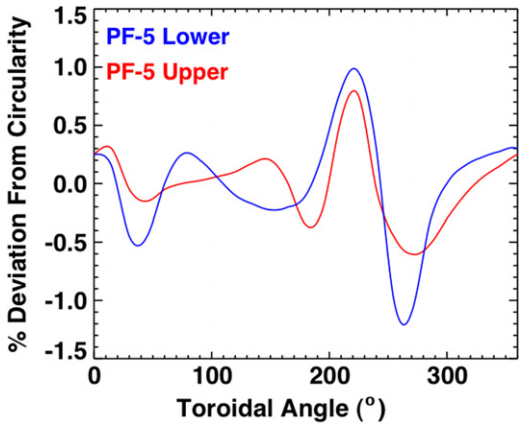

Figure 5. Fractional deviation of the upper and lower PF-5 coils from circularity; see text for additional details.

profiles of the $n = 3$ amplitude match best with ~18.5 A in the EFC coils per 1 kA of current in the PF-5 coil. The amplitude and phase of the optimal matching field are shown in figures 6(*a*) and (*b*). The radial profiles of the $n = 3$ amplitudes are shown in figure 6(*c*); an excellent fit to the radial profile is achieved. The optimal correction is the opposite of this matching field, and is thus approximately $I_{EFC,1}/I_{PF\text{-}5} = -18.5\,A\,kA^{-1}$, which is essentially consistent with the experimental correction of $I_{EFC,1}/I_{PF\text{-}5} = -14\,A\,kA^{-1}$. Note the small $n = 9$ sideband in the spectrum of the EFC coil in figures 6(*a*) and (*c*).

The correction is not, however, perfect. As shown in figure 6(*b*), the phase of the $n = 3$ source and correction fields is not perfectly matched; they differ by ~20°. However, with only six correction coils, the $n = 3$ phase cannot be further optimized. Additionally, the EFC coils, when configured to make $n = 3$ fields, also create an $n = 9$ sideband component noted above; this sideband can create additional NTV braking [28], and is thus undesirable. Finally, the poloidal spectrum of the error and correction fields will differ, even for perfectly toroidally aligned $n = 3$ fields at the midplane. A correction coil set with more than six coils, and with a poloidal distribution of coils, could in principle further improve the correction.

We have also computed the NTV torque expected from the vertical field coil non-circularity and correcting fields. These calculations use the Ideal Perturbed Equilibrium Code (IPEC) [24, 38] to model the plasma response to the perturbations, and a generalized NTV theory [37] to calculate the NTV torque.

The IPEC code solves the perturbed ideal MHD force balance equation,

$$\vec{F} = 0 = \vec{\nabla}\delta p - \delta\vec{j} \times \vec{B}_0 - \vec{j}_0 \times \delta\vec{B}_0, \tag{5}$$

subject to the constraint that the resonant magnetic perturbation at each rational surface vanishes. This constraint is met by calculating appropriate shielding currents at the rational surfaces. The resulting ideal equilibrium can have magnetic surfaces with significant 3D shape variations. More details regarding the IPEC code can be found in [24, 38].

The magnetic equilibrium used in the IPEC code is then used to calculate the NTV damping, using the formulation described in [24, 37]. Many previous calculations of NTV rely on formulations for two separate collisionality regimes: the $1/\nu$ regime for $\omega_E \ll \nu$, and the $\nu - \nu^{1/2}$ regime for $\omega_E \gg \nu$ (here, ω_E is the toroidal $E \times B$ procession frequency) [24]. However, many tokamaks, including NSTX, reside in a parameter space between these two regimes. The present NTV formulation smoothly connects the regimes, eliminating the

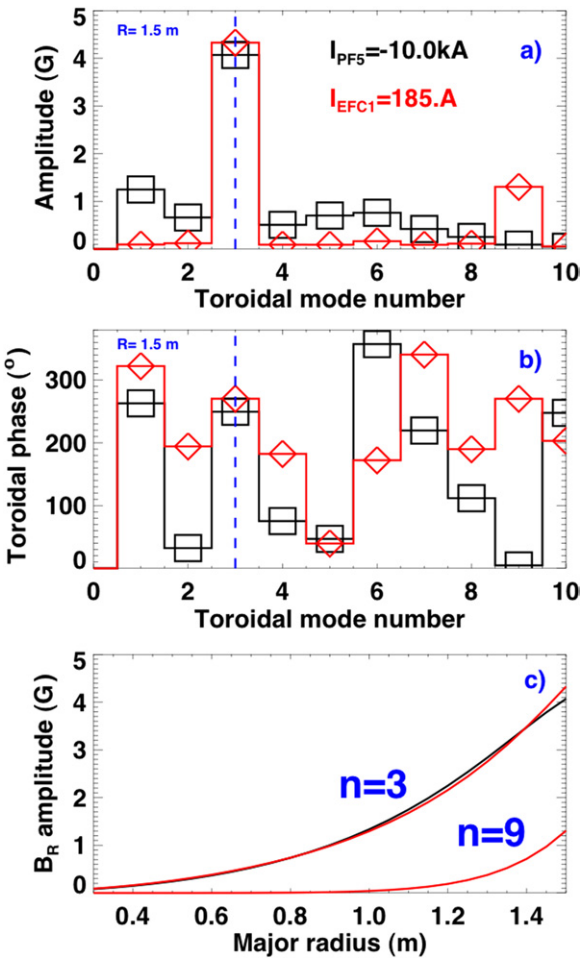

Figure 6. Assessment of the vacuum EF, and $n = 3$ field which would compensate it. Shown are the midplane (a) amplitude and (b) phase spectra of the EF from the PF-5 coils, as well as the vacuum fields from the EFC coil configuration that approximately matches the EF. Also shown are the vacuum radial profiles of the $n = 3$ fields, and the $n = 9$ sideband from the EFC coils.

ambiguity of which to choose. It also includes multi-harmonic calculations of resonance effects between the electric precession and bounce orbits.

The results of these NTV calculations are shown in figure 7, for the experimental case with $I_P = 1100$ kA and $B_T = 0.55$ T, where the vertical field coil had about 10 kA during the time of interest. The NTV calculation requires the total magnetic field on the magnetic surface to be specified as $B = B_0(1 - \varepsilon \cos\theta) + \delta B$. The perturbation field δB comes from two sources: the vertical field coil, whose current is set to be 10 kA, and the EFC coil, whose current is scanned in repeated calculations to make the figure. The calculation in figure 7(a) shows the net NTV torque without a calculation of the plasma response, i.e. without the self-consistent distortion of the magnetic surfaces. Here, the field variation δB in the NTV calculation for this case is the Eulerian variation at a fixed point, $\delta_E B^x = \delta \vec{B}^x \cdot \vec{B}_0$. The calculation does indeed show a minimum in the torque at correction currents of ~ -200 A (for 10 kA in PF-5). However, the magnitude of the torque is too small by ~ 2 orders of magnitude. This underestimation

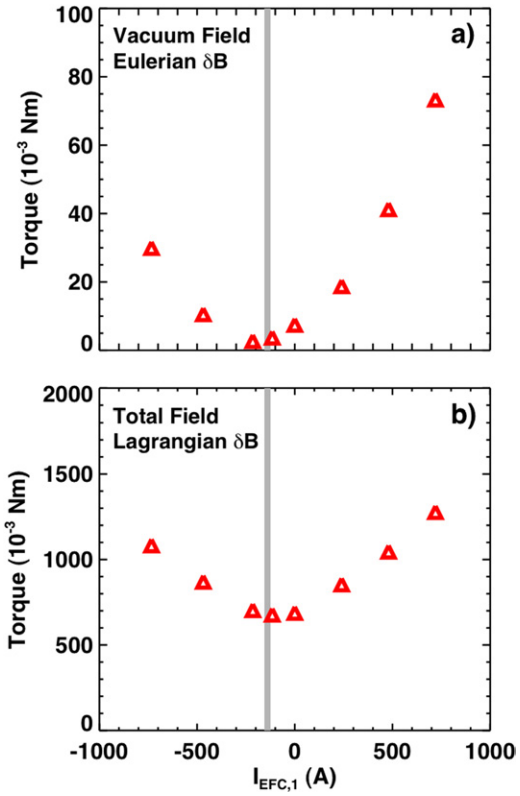

Figure 7. Calculation of the total NTV torque (EF and applied field) as a function of the $n = 3$ applied field amplitude and polarity, for the scan at $I_P = 1100$ kA and $B_T = 0.55$ T. The calculation in (*a*) is based on only the vacuum superposition, while that in (*b*) considers the total plasma response in calculating the field variations; see text for additional details.

of the NTV torque while using the Eulerian field variation has been noted previously in [24].

The same calculation, but using the 3D equilibrium from IPEC and the full Lagrangian formulation for δB, is shown in figure 7(*b*). In this Lagrangian formulation, the local field variation is given by $\delta_L B = \delta\vec{B} \cdot \vec{B}_0 + \vec{\xi} \cdot \vec{B}_0$, and hence accounts for variations in field strength along the field line due to changes in both the 3D field magnitude and the field line trajectories [24, 46]. Once again, the optimal correction is displaced toward negative values for coil 1, consistent with all previously shown results; the optimal correction in this case is found to be in the vicinity of $I_{EFC,1}/I_{PF\text{-}5} \approx -13$ A kA^{-1}.

Additionally, note that the magnitude of the torque is approximately correct in figure 7(*b*). For instance, in figure 2(*g*), the angular momentum changes by ≈0.05 J s in a duration of ≈0.1 s when the EFC coils are energized at the 750 A level; the inferred change in torque is thus 0.5 N m. This is consistent (within a factor of 2) with the *change* in torques predicted by the IPEC + generalized NTV formulation. As described in [24], the NTV calculation is generally only accurate to within this accuracy; further refinements to the theory are necessary in order to refine these comparisons. We also note that the torque does not go to zero due to the imperfect match between the applied field spectrum and EF spectrum.

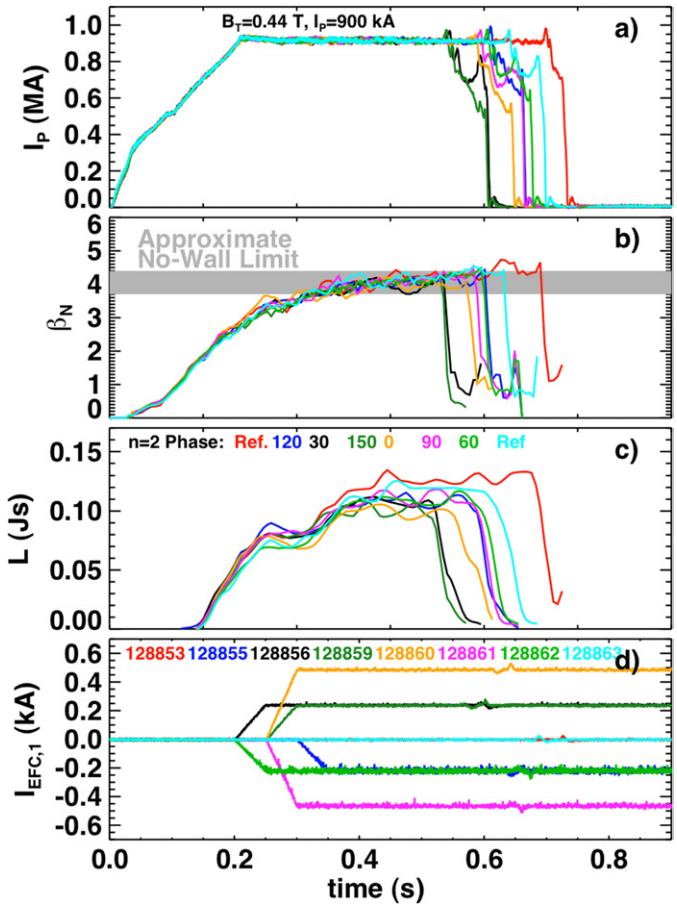

Figure 8. Time evolution of a series of discharges used to look for $n = 2$ EFs. Shown are (*a*) the plasma current, (*b*) the normalized β value, (*c*) the plasma angular momentum and (*d*) the current in EFC coil 1.

5. Measurements of $n = 2$ EFs in NSTX

The experimental measurement and correction of the $n = 3$ EF motivated a search for $n = 2$ non-resonant EFs. The typical midplane field pattern in the $n = 2$ configuration is shown in figure 1(*c*). While the $n = 2$ component is the largest term, there are large sidebands. For instance, the outboard midplane value of the $n = 4$ component is ∼60% of the $n = 2$ component amplitude, while the $n = 8$ component is about 20%. Given the n^2 dependence of the NTV torque, these higher order terms can also be very important.

An experiment similar to those described in section 3 was conducted in order to assess the presence of $n = 2$ EFs in NSTX. The results from a representative experiment are shown in figure 8. The phases of the $n = 2$ field are indicated in the text in figure 8(*c*), where 'Ref.' indicates that no $n = 2$ fields were applied. In each case, the maximum current in any EFC coil was 500 A. The two reference shots develop an RWM at ∼0.7 s; the application of $n = 2$ fields leads to a shortening of the shot in all cases. The angular momentum of the plasma is also reduced in each case with applied $n = 2$ fields; the reference shots with no applied fields have the largest angular momentum. The phase scan in this experiment was repeated for cases with

both 250 and 750 A as the maximum current in any EFC coil. For the 250 A case, the braking was observed for all phases, although without a significant impact on the shot duration. In the 750 A case, the braking was larger in all cases, and the shot duration severely reduced.

This uniformity of the plasma response to the $n = 2$ fields of various phases implies that $n = 2$ EFs are likely small in NSTX. This confirms our picture of the vertical field coil EF source, which is calculated in figure 6(*a*) to have only small $n = 2$ components. This conclusion must be treated with some caution, however, due to two considerations. First, the $n = 4$ and 10 sidebands of the applied fields, which are unavoidable given the NSTX EFC coil geometry, might produce additional magnetic braking that would cancel the beneficial effect of $n = 2$ EF correction. Second, any $n = 2$ fields which do not couple strongly to the fields from the EFC coils would not be properly corrected by the scans in this experiment.

6. Summary

In this paper, we have shown that the detection and correction of non-resonant EFs can be an important element in improving the performance of a tokamak. The asymmetric response of the plasma to $n = 3$ fields of varying phases demonstrates that an intrinsic $n = 3$ EF is present in NSTX; correcting this EF can lead to improved performance at high β_N. Repeating this experiment for various values of I_P, B_T and elongation has enabled the conclusion that the main vertical field coil (PF-5) is the source of the EF. This is confirmed by analysis of the coil shape, which does indeed have an $n = 3$ radial modulation. The optimal correction for the field from this distortion is calculated from two different perspectives: the vacuum correction field that best cancels the vacuum EF, and the correction field that results in a minimal NTV braking. The two methods generally agree with each other, and with the experimentally determined optimal correction. Experiments designed to study $n = 2$ EFs, however, were unable to find an asymmetric response as the applied field phase was changed. This implies that $n = 2$ EFs, if present in NSTX, are likely small enough to not impact plasma performance.

The results from this and other works imply that future tokamaks and spherical torii should have the ability to apply and correct $n > 1$ EFs. EF strategies for ITER [47], for instance, have focused on $n = 1$ EFs [48]. These studies should be expanded to include likely sources of $n > 1$ EFs, detection methods and mitigation strategies.

Acknowledgments

This work was funded by the United States Department of Energy contract DE-AC02-09CH11466. The authors would like to thank Dennis Mueller, Roger Raman and Tim Stevenson for the skillful operation of NSTX for these experiments.

References

[1] La Haye R J and Scoville J T 1991 *Rev. Sci. Instrum.* **62** 2146
[2] Fitzpatrick R 1993 *Nucl. Fusion* **33** 1049
[3] Lazzaro E *et al* and Contributors to the EFDA-JET Work Programme 2002 *Phys. Plasmas* **9** 3906
[4] Cole A J, Hegna C C and Callen J D 2007 *Phys. Rev. Lett.* **99** 065001
[5] Cole A J, Hegna C C and Callen J D 2008 *Phys. Plasmas* **15** 056102
[6] Scoville J T, La Haye R J, Kellman A G, Osborne T H, Stambaugh R D, Striat E J and Taylor T S 1991 *Nucl. Fusion* **31** 875
[7] Hender T *et al* 1992 *Nucl. Fusion* **32** 2091
[8] La Haye R J, Hyatt A W and Scoville J T 1992 *Nucl. Fusion* **32** 2119
[9] La Haye R J, Fitzpatrick R, Hender T C, Morris A W, Scoville J T and Todd T N 1992 *Phys. Fluids* B **4** 2098

[10] Fishpool G M and Haynes P S 1994 *Nucl. Fusion* **34** 109
[11] Buttery R J *et al*, JET Team, COMPASS-D Research Team and DIII-D Team 1999 *Nucl. Fusion* **39** 1827
[12] Buttery R J, De'Benedetti M, Hender T C and Tubbing B J D 2000 *Nucl. Fusion* **40** 807
[13] Scoville J T and La Haye R J 2003 *Nucl. Fusion* **43** 250
[14] Wolfe S M *et al* 2005 *Phys. Plasmas* **12** 056110
[15] Menard J E *et al* and the NSTX Research Team 2010 Progress in understanding error-field physics in NSTX spherical torus plasmas *Nucl. Fusion* at press
[16] Boozer A H 2001 *Phys. Rev. Lett.* **86** 5059
[17] Troyon F, Gruber R, Saurenmann H, Semenzato S and Succi S 1984 *Plasma Phys. Control. Fusion* **26** 209
[18] Strait E J 1994 *Phys. Plasmas* **1** 1415
[19] Garofalo A M *et al* 2002 *Phys. Plasmas* **9** 1997
[20] Reimerdes H *et al* 2006 *Phys. Plasmas* **13** 056107
[21] Reimerdes H *et al* 2009 *Nucl. Fusion* **49** 115001
[22] Sabbagh S A *et al* 2006 *Nucl. Fusion* **46** 635
[23] Park J-K, Schaffer M J, Menard J E and Boozer A H 2007 *Phys. Rev. Lett.* **99** 195003
[24] Park J-K, Boozer A H, Menard J E, Garofalo A M, Schaffer M J, Hawryluk R J, Kaye S M, Gerhardt S P, Sabbagh S A and NSTX Team 2009 *Phys. Plasmas* **16** 056115
[25] Evans T E *et al* 2006 *Nature Phys.* **2** 419
[26] Evans T E *et al* 2008 *Nucl. Fusion* **48** 024002
[27] La Haye R J, Günter S, Humphreys D A, Lohr J, Luce T C, Maraschek M E, Petty C C, Prater R, Scoville J T and Strait E J 2002 *Phys. Plasmas* **9** 2051
[28] Zhu W *et al* 2006 *Phys. Rev. Lett.* **96** 225002
[29] Garofalo A M, Burrell K H, DeBoo J C, deGrassie J S, Jackson G L, Lanctot M, Reimerdes H, Schaffer M J, Solomon W M and Strait E J 2008 *Phys. Rev. Lett.* **101** 195005
[30] Garofalo A M *et al* 2009 *Phys. Plasmas* **16** 056119
[31] Sabbagh S A *et al* 2010 *Nucl. Fusion* **50** 025020
[32] Shaing K C 1983 *Phys. Fluids* **26** 3315
[33] Shaing K C 2003 *Phys. Plasmas* **10** 1443
[34] Shaing K C, Cahyna P, Becoulet M, Park J-K, Sabbagh S A and Chu M S 2008 *Phys. Plasmas* **15** 082506
[35] Shaing K C, Sabbagh S A and Chu M S 2009 *Plasma Phys. Control. Fusion* **51** 035009
[36] Shaing K C, Sabbagh S A and Chu M S 2009 *Plasma Phys. Control. Fusion* **51** 055003
[37] Park J-K, Boozer A H and Menard J E 2009 *Phys. Rev. Lett.* **102** 065002
[38] Park J-K, Boozer A H and Glasser A H 2007 *Phys. Plasmas* **14** 052110
[39] Solomon W H, Kaye S M, Bell R E, LeBlanc B, Levington F M, Menard J E, Rewalt G, Sabbagh S A, Wang W and Yuh H 2008 *Phys. Rev. Lett.* **101** 065004
[40] Kaye S M, Solomon W, Bell R E, LeBlanc B P, Levinton F, Menard J, Rewoldt G, Sabbagh S, Wang W and Yuh H 2009 *Nucl. Fusion* **49** 045010
[41] Solomon W M *et al* 2010 Mechanisms for generating toroidal rotation in tokamaks without external momentum input *Phys. Plasmas* at press
[42] Ono M *et al* and the NSTX Team 2000 *Nucl. Fusion* **40** 557
[43] Wesson J 1997 *Tokamaks* (Oxford: Clarendon)
[44] Sontag A C *et al* 2007 *Nucl. Fusion* **47** 1005
[45] Sabbagh S A, Bell R E, Menard J E, Gates D A, Sontag A C, Bialek J M, LeBlanc B P, Levinton F M, Tritz K and Yuh H 2006 *Phys. Rev. Lett.* **97** 045004
[46] Gerhardt S P, Anderson D T and Talmadge J N 2005 *Phys. Plasmas* **12** 012504
[47] Hender T C *et al* and the ITPA MHD, Disruption and Magnetic Control Topical Group 2007 *Nucl. Fusion* **47** S128
[48] Park J-K, Boozer A H, Menard J E and Schaffer M J 2008 *Nucl. Fusion* **48** 045006